Eur. Phys. J. D (2020) 74: 105
https://doi.org/10.1140/epjd/e2020-10036-5

THE EUROPEAN PHYSICAL JOURNAL D

Regular Article

Molecular-frame (e, 2e) ionization dynamics of H_2 at high impact-energy

Enliang Wang[1,a], Esam Ali[2], Xingyu Li[3,4], Xueguang Ren[1,5,b], Xiangjun Chen[3,4], Don Madison[2], and Alexander Dorn[1]

[1] Max-Planck-Institut für Kernphysik, Heidelberg 69117, Germany
[2] Department of Physics, Missouri University of Science and Technology, Rolla, MO 65409, USA
[3] Hefei National Laboratory for Physical Sciences at Microscale and Department of Modern Physics, University of Science and Technology of China, Hefei, Anhui 230026, P.R. China
[4] Synergetic Innovation Center of Quantum Information and Quantum Physics, University of Science and Technology of China, Hefei, Anhui 230026, P.R. China
[5] School of Science, Xi'an Jiaotong University, Xi'an 710049, P.R. China

Received 17 January 2020 / Received in final form 31 March 2020
Published online 28 May 2020

Abstract. We report a combined experimental and theoretical study on the electron-impact ionization dynamics of H_2 at an impact-energy of 520 eV. The molecular-frame fivefold-differential cross sections were measured for electron emission in the plane perpendicular to the incoming projectile beam. An (e, 2e + ion) triple coincidence method was used covering projectile scattering angles of 6.5°, 10.0° and 20.0° and ejected energies of 20 eV and 30 eV. The experimental cross sections are compared with results from the multi-center distorted-wave (MCDW) as well as the molecular three-body distorted wave (M3DW) approaches. M3DW is in overall better agreement with the measured data in the binary lobes than MCDW, while the intensity of recoil lobes are underestimated by both theories. Furthermore, we examine the presence of two-center interference patterns by comparing the experimental cross section ratios between mutually perpendicular alignment angles of the molecular axis with that predicated by the interference model. Agreement with the interference model is found only for Bethe ridge kinematics, i.e. in the binary peak region and with the ejected electron momentum being roughly equal to the momentum transfer. Finally, we suggest a modified interference formula for the recoil peak which takes into account the backscattering of the ejected electron in the ionic potential.

1 Introduction

Collisions of electrons with atoms and molecules are of critical importance for a wide range of scientific and practical applications, e.g. for the understanding of quantum many-body dynamics and the modeling of plasma, astrophysical processes, as well as ionizing radiation in biological systems [1,2]. Single ionization of the target is one of the most important types of collisions and the best way to study this process is through the so-called (e, 2e) experiment which comprehensively characterizes the outcome of the many-body dynamics. This is a kinematically complete experiment, in which the linear momentum vectors of all final-state particles are determined [3,4].

In recent years, theory has made tremendous progress in describing the ionization dynamics, e.g. the basic three-body problem was claimed to be numerically solved in electron-impact ionization of atomic hydrogen (H) by non-perturbative theories [5–7]. It is also considered to be well understood for ionization of lighter atoms beyond H, like helium and neon while for heavier systems like argon, agreement is still not quantitative [8–14].

For molecules, it becomes even more challenging to understand the collision dynamics due to the multi-center nature, the more complex electronic structure and the difficulty of determining the molecular orientation experimentally [15–18]. Here, electron scattering on the smallest molecules like H_2 is of fundamental importance to benchmark theory, see e.g. references [19,20]. An interesting aspect of electron collisions with targets containing several scattering centers are interference effects. For molecular hydrogen, a number of existing studies for ion and electron impact ionization have identified interference patterns in the ejected electron energy distribution or angular distribution which can be described in analogy with the Young's double-slit experiment performed with light (see e.g. [21–29]).

[a] e-mail: enliang.wang@mpi-hd.mpg.de
[b] e-mail: ren@mpi-hd.mpg.de

The close relation of particle impact ionization to the interference pattern observed for emission from two coherent light sources (double-slit) is seen if some approximations are made for the description of impact ionization. These are, firstly, the treatment of the incoming and scattered projectile as plane waves and, secondly, the description of the ionized electron as a superposition of spherically symmetric Coulomb waves emitted from each atomic center within the molecule. As result the (e, 2e) fivefold-differential cross section (5DCS) for diatomic molecules like H_2 can be expressed as [30]:

$$\sigma_{H_2} = \frac{d\sigma_{H_2}}{d\theta_m d\phi_m d\Omega_1 d\Omega_2 dE_2} = 2\sigma_H \cdot \left[1 + \cos\left(\vec{k}_2 \cdot \vec{R} - \vec{q} \cdot \vec{R}\right)\right], \quad (1)$$

where θ_m and ϕ_m represent the direction of molecular alignment, Ω_1 and Ω_2 represent the solid angles of the scattered projectile and ejected electron, respectively [31]. σ_H is the atomic (one-center) differential cross section. $\left[1 + \cos\left(\vec{k}_2 - \vec{q}\right) \cdot \vec{R}\right]$ is referred to as the interference factor. $\vec{k}_2$, $\vec{q}$ and $\vec{R}$ are the ejected electron momentum, the momentum transferred by the scattered projectile and the internuclear vector of H_2, respectively. In equation (1), the phase $\vec{k}_2 \cdot \vec{R}$ is due to the path difference of the waves emitted from the two centers. $\vec{q} \cdot \vec{R}$ is the phase difference of the incoming and outgoing projectile waves relative to the two centers and $\vec{k}_2 - \vec{q}$ coincides with the recoil ion momentum.

Most of the existing (e, 2e) studies concerning Young-type interference for diatomic molecules were obtained without knowing the molecular spatial alignment and, therefore, they represent an average over all angles Ω_m, see e.g. [29,32–35]. Molecular-frame (e, 2e) experiments where this averaging is not done and which can give better insight into observed cross section oscillations are well suited to verifying the two-center interference in electron-impact ionization of molecules [29]. Using the coincident detection of protons from molecular hydrogen dissociation, we were able to obtain molecular frame (e, 2e) data [31]. In a recent study for $E_0 = 520\,\text{eV}$, we found strong molecular alignment dependent cross sections for low-energy electron emission of $E_2 = 10\,\text{eV}$ [36]. Since the electron emission pattern was in strong disagreement with the predictions of the interference model, we concluded that the underlying approximations are not applicable at low energy. In particular, it appears that the treatment of the ejected electron as the superposition of undisturbed spherical waves neglecting the two-center character of the ionic potential is not valid.

In the present work, we extend our molecular-frame (e, 2e) study for $E_0 = 520\,\text{eV}$ to higher energies of the ejected electron of $E_2 = 20\,\text{eV}$ and $30\,\text{eV}$. Consequently, the influence of the ionic multi-center potential on the outgoing wave should be reduced compared to the earlier studied $E_2 = 10\,\text{eV}$. It is also to be noted that ionized electron energies of $20\,\text{eV}$ and higher can be produced only by direct impact ionization while, for lower energies, contributions from doubly excited autoionizing states cannot be fully excluded [17,37]. Additionally, we introduce a new way to analyze the data by studying the 5DCS ratio for two mutually perpendicular alignment angles of the molecular axis. This will be elucidated in the following.

According to the interference model in equation (1), the 5DCS of H_2 is proportional to the atomic cross section σ_H multiplied by the interference factor $1+\cos\left[\left(\vec{k}_2 - \vec{q}\right) \cdot \vec{R}\right]$. Thereby, if we take a cross section ratio between two different molecular alignments, the atomic cross section cancels completely. This removes any possible ambiguity or uncertainty related to the determination of the atomic cross section and leads to a pure ratio of interference factors for the (e, 2e) reaction:

$$\tilde{R} = \frac{\sigma_{H_2}(\phi_m = 0°)}{\sigma_{H_2}(\phi_m = 90°)} = \frac{1 + \cos\left[\left(\vec{k}_2 - \vec{q}\right) \cdot \vec{R}_{\phi_m = 0°}\right]}{1 + \cos\left[\left(\vec{k}_2 - \vec{q}\right) \cdot \vec{R}_{\phi_m = 90°}\right]}. \quad (2)$$

Comparing this ratio with the respective experimental result clearly reveals if Young's double slit interference can be observed for the present system.

2 Experimental method

The experiment was performed using a reaction microscope designed for electron impact studies which was described in detail elsewhere [31,38,39]. Briefly, a well-focused pulsed electron beam intersects a supersonic cold H_2 gas jet. Using uniform electric and magnetic fields, the final-state charged particles (electrons and ions) were extracted into opposite directions and projected onto two position- and time-sensitive multi-hit detectors. From the positions of the hits and their times-of-flights, the initial momentum vectors of the particles can be reconstructed. The molecular alignment was determined from ground state dissociation (GSD) of the H_2^+ cation where the molecular ion in its electronic ground state dissociates into a hydrogen atom and a proton [40]. While ionization of H_2 most likely leads to the vibrational excited electronic ground state of H_2^+ a small initial internuclear separation around $R = 1.1$ a.u. can lead to the vibrational continuum of the same electronic state followed by dissociation. Based on the axial recoil approximation (ARA) [41], the alignment of the molecular axis can be determined from the momentum vector of the proton. In fact, the lab frame momentum vector of the proton includes two parts: (i) the momentum from dissociation, and (ii) the collisional recoil momentum. The latter one was subtracted and only the momentum from dissociation was used to determine the molecular orientation as described by Senftleben et al. [31]. To fulfill the preconditions of the ARA, small proton momenta were excluded and a momentum range from 3 to 10 a.u. was used for the analysis. The perpendicular plane geometry was selected by requesting the ejected electron emission within $90° \pm 15°$ with respect to the incoming beam direction. The molecular axis is also within the same plane. For a particular orientation angle, the apex angle of the allowance cone was $\pm 20°$. The acceptance region of scattering angles and slow electron energies

are: $\theta_1 = 6.5 \pm 1°$, $10 \pm 2°$ and $20 \pm 3°$, and $E_2 = 20 \pm 3\,\text{eV}$ and $30 \pm 3.5\,\text{eV}$.

3 Theoretical method

The multi-center distorted-wave (MCDW) as well as the molecular three-body distorted wave (M3DW) calculations were performed at a fixed internuclear separation of $R = 1.1\,\text{a.u.}$ to precisely consider the GSD condition of H_2^+. The details about theoretical methods have been described previously in references [42,43] for MCDW and references [44–46] for M3DW. Briefly, the MCDW method is developed within the framework of the first Born approximation (FBA) in which the continuum wave function of the slow ejected electron is calculated in the spatially fixed multi-center potential of the residual ion under the sudden approximation and plane waves are adopted to describe the incident and scattered projectile. In the scattering theory, the transition amplitude for a given molecular orientation in the laboratory can be expressed as:

$$T_{fi}(\Omega) = \left\langle \boldsymbol{k}_1 \Psi_f^{(-)}(\boldsymbol{k}_2; \mathcal{R}_\Omega^{-1}(\boldsymbol{r}))\, |V|\, \boldsymbol{k}_0 \Psi_i\left(\mathcal{R}_\Omega^{-1}(\boldsymbol{r})\right) \right\rangle \quad (3)$$

$|\boldsymbol{k}_0\rangle$ and $|\boldsymbol{k}_1\rangle$ describe the plane waves of the incident and scattered electrons with momentum $\boldsymbol{k}_0$ and $\boldsymbol{k}_1$, respectively. $\boldsymbol{k}_2$ is the momentum vector of the ejected electron. $|\Psi_i\rangle$ and $\left|\Psi_f^{(-)}\right\rangle$ represent the initial bound wave function and the final state in which the ionized orbital is substituted by the continuum wave function of the ejected electron. A specific spatial alignment of the molecular axis within the coordinate system chosen to represent the collision kinematics is achieved by rotating the molecular wave function with the operator $\mathcal{R}_\Omega^{-1}$. Here $\Omega = (\alpha, \beta, \gamma)$ are the Euler angles and $\boldsymbol{r}$ refers to the set of electronic coordinates with respect to the center of mass of molecule. $V = \sum_i^N \frac{1}{|\boldsymbol{r}_i - \boldsymbol{r}_0|} - \sum_n \frac{Z_n}{|\boldsymbol{R}_n - \boldsymbol{r}_0|}$ is the interaction potential of incident electron and the molecular target where $\boldsymbol{r}_i$ and $\boldsymbol{r}_0$ are the position vectors of the ith bound electron of the molecular target and incident electron, respectively and $\boldsymbol{R}_n$ represents the position of the nth nucleus and Z_n is the corresponding nuclear charge. With the help of Bethe integral [47,48] integration over the projectile coordinate $\boldsymbol{r}_0$ is carried out and equation (3) can be simplified as an one electron problem. Under the frozen core approximation in which the wave function of the remaining bound electron is the same in the initial and final states one obtains:

$$T_{fi}(\Omega) \sim \left\langle \mathcal{F}^{(-)}(\boldsymbol{k}_2; \mathcal{R}_\Omega^{-1}(\boldsymbol{r})) \left| e^{i\boldsymbol{q}\cdot\boldsymbol{r}} - \sum_{n=a,b} \frac{e^{i\boldsymbol{q}\cdot\boldsymbol{r}_n}}{2} \right| \phi(\boldsymbol{r}_a) + \phi(\boldsymbol{r}_b) \right\rangle \quad (4)$$

where $\mathcal{F}^{(-)}$ is the continuum wave function of the ejected electron which is solved under the two-center field of the H_2^+ ion. The term $e^{i\boldsymbol{q}\cdot\boldsymbol{r}}$ represents the scattering from the active electron in the target and the term $\Sigma_{n=a,b} e^{i\boldsymbol{q}\cdot\boldsymbol{r}_n}/2$ represents the scattering from the nuclei. $\vec{q} = \vec{k}_0 - \vec{k}_1$ is the projectile momentum transfer to the target. In the above expression, we use the linear combination of atomic orbitals (LCAO) approximation in writing the wave function of the initial bound molecular orbital, $\phi(\boldsymbol{r}_a) + \phi(\boldsymbol{r}_b)$. In the actual calculation, the atomic orbital is expanded by basis sets and the coefficients of the basis functions for molecular orbital are determined by a self-consistent field calculation performed by quantum chemistry software, i.e. Gaussian package [49]. The transition amplitude can thus be written as the sum of two one-center amplitudes:

$$T(\Omega) \sim A_a e^{i\theta_a} + A_b e^{i\theta_b}, \quad (5)$$

where

$$A_a e^{i\theta_a} \sim \left\langle \mathcal{F}^{(-)}(\boldsymbol{k}_2; \mathcal{R}_\Omega^{-1}(\boldsymbol{r})) \left| e^{i\boldsymbol{q}\cdot\boldsymbol{r}} - \sum_{n=a,b} \frac{e^{i\boldsymbol{q}\cdot\boldsymbol{r}_n}}{2} \right| \phi(\boldsymbol{r}_a) \right\rangle, \quad (6)$$

$$A_b e^{i\theta_a} \sim \left\langle \mathcal{F}^{(-)}(\boldsymbol{k}_2; \mathcal{R}_\Omega^{-1}(\boldsymbol{r})) \left| e^{i\boldsymbol{q}\cdot\boldsymbol{r}} - \sum_{n=a,b} \frac{e^{i\boldsymbol{q}\cdot\boldsymbol{r}_n}}{2} \right| \phi(\boldsymbol{r}_b) \right\rangle. \quad (7)$$

Here A_a and A_b represent the magnitudes of the one-center amplitudes, and θ_a and θ_b are their phases. The transition amplitude equation (5) is related to the differential cross section by

$$\sigma = |T|^2 = A_a^2 + A_b^2 + 2A_a A_b \cos(\theta_a - \theta_b). \quad (8)$$

There are two direct terms, A_a^2 and A_b^2, which correspond to the cross section of the individual atoms, and a cross term $2A_a A_b \cos(\theta_a - \theta_b)$. As mentioned in earlier works [42,43], the diagonal terms in the potential matrix are considered to be dominant. Thus, in computations we will ignore the off-diagonal elements and solve the decoupled partial wave equations.

For the M3DW calculation, all continuum waves are described by distorted waves. The distorted waves are a solution of the Schrödinger equation using a spherically symmetric distorting potential for the neutral H_2 molecule (incident channel) or singly ionized H_2^+ molecular ion (final channel). This distorting potential is a spherical averaged multi-center potential which is a sum of the contributions from the electronic part and the nuclear part. The electronic part is calculated using the numerical charge density obtained from the orbitals calculated using density functional theory. For the nuclear part, a spherical average of two protons located a distance of 0.55 a.u. from the center-of-mass places a charge of +2 on a thin spherical shell which has a radius of 0.55 a.u. This potential is multi-center in the sense that it takes the proper charge density and location of the nuclei into account, but, in the averaging process, it does not depend on the exact orientation of the molecule. The distorted wave used in the MCDW approximation, on the other hand, does depend on the orientation of the molecule. In

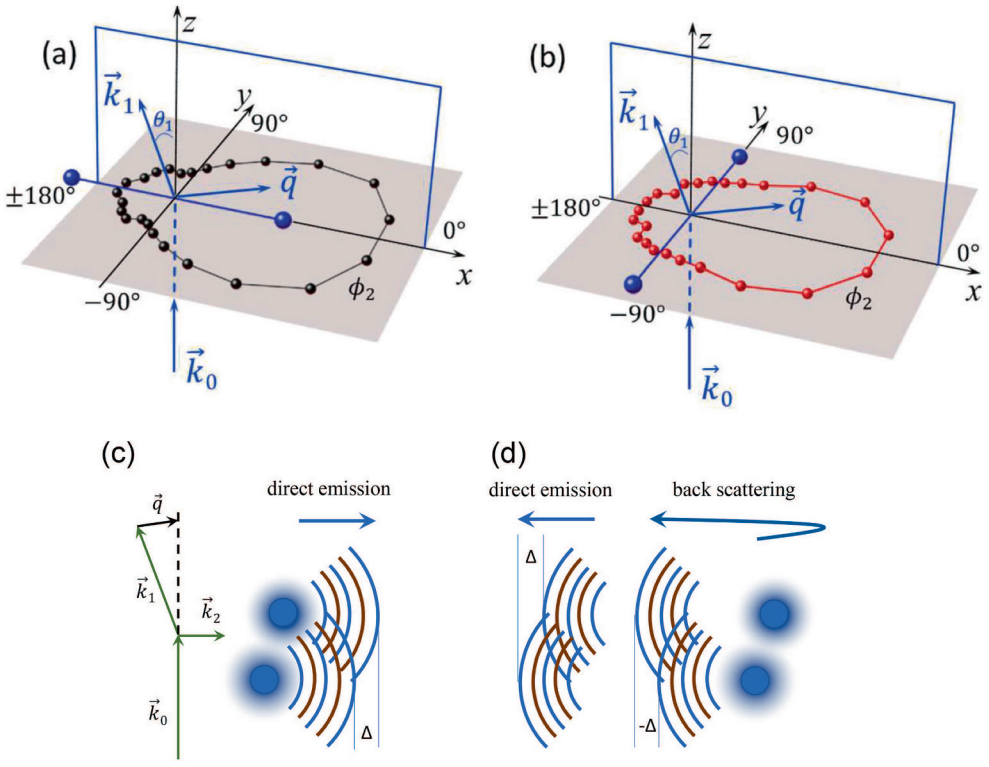

Fig. 1. Molecular-frame (e, 2e) cross section in the perpendicular plane as polar plots for the scattering angle $\theta_1 = 6.5°$ and ejected energy $E_2 = 20\,\text{eV}$. The (blue) spheres indicate the H_2 molecular axis which is aligned in the same plane and with $\phi_m = 0°$ for (a) and $\phi_m = 90°$ for (b). The sketches on the bottom show the collision kinematics of binary (c) and recoil mechanisms (d). The backscattering of recoil ion potential to emitted electron will change the emitted phase in the interference factor.

the M3DW, the orientation of the molecule is contained in the initial bound state wave function. One of the primary strengths of the M3DW approach lies in the fact that it treats the final state Coulomb interaction between the scattered and ejected electrons exactly (normally called post-collision interaction PCI) while the MCDW method does not contain PCI. PCI should be important when the scattered and ejected electrons have similar energies (speeds). However, for the kinematics of this experiment, there is a large difference between the energies of the scattered and ejected electrons so PCI is probably not very important.

4 Results and discussion

As illustrated in Figures 1a and 1b, we measured electron emission in a plane perpendicular to the projectile beam axis. The incoming projectile ($\vec{k}_0$) enters from the bottom and after the collision, it will most likely be the fast outgoing electron which we define to be scattered to the left ($\vec{k}_1$) with scattering angle θ_1. The projectile momentum transfer to the target is indicated by $\vec{q} = \vec{k}_0 - \vec{k}_1$. The projectile scattering angles are $\theta_1 = 6.5°$, 10° and 20° giving rise to momentum transfer values $|\vec{q}|$ of approximately 0.7 a.u., 1.1 a.u. and 2.1 a.u., respectively. The ionized electron energies were $E_2 = 20\,\text{eV}$ and 30 eV corresponding to electron momentum values of 1.2 a.u. and 1.5 a.u. This includes kinematics where the momentum transfer is smaller, roughly equal to, and larger than the ejected electron momentum. Thus, different regions of the bound state momentum profile are probed in the experiment. (e, 2e) cross sections of H_2 are obtained for two different orientations of the molecular axis within the perpendicular plane. In Figures 1a and 1b, the H_2 molecular alignment is indicated by the (blue) spheres in the plots. Panels (a) and (b) show the results for molecular alignments ($\theta_m = 90°$, $\phi_m = 0°$) and ($\theta_m = 90°$, $\phi_m = 90°$). Here θ_m and ϕ_m are the polar angle of the molecular axis and the azimuthal angle with respect to the x-axis, respectively. The x-axis is defined as the intersection line of the projectile scattering plane and the perpendicular plane (see Fig. 1).

The cross section data in Figures 1a and 1b obtained for $\theta_1 = 6.5°$, $E_2 = 20\,\text{eV}$ display the principal features of the electron emission pattern: it is governed by the well-known binary and recoil lobes. The binary lobe in the $+x$ direction ($\phi_2 \sim 0°$) is oriented roughly along the direction of the momentum transfer $\vec{q}$, as schematically shown in Figure 1c. This corresponds to electrons emitted after a single binary collision with the projectile. In the opposite direction ($\phi_2 \sim \pm 180°$), the much weaker recoil lobe is found, which is attributed to a binary collision followed by backscattering in the nuclear potential resulting in emission roughly in the direction of $-\vec{q}$, as schematically shown in Figure 1d.

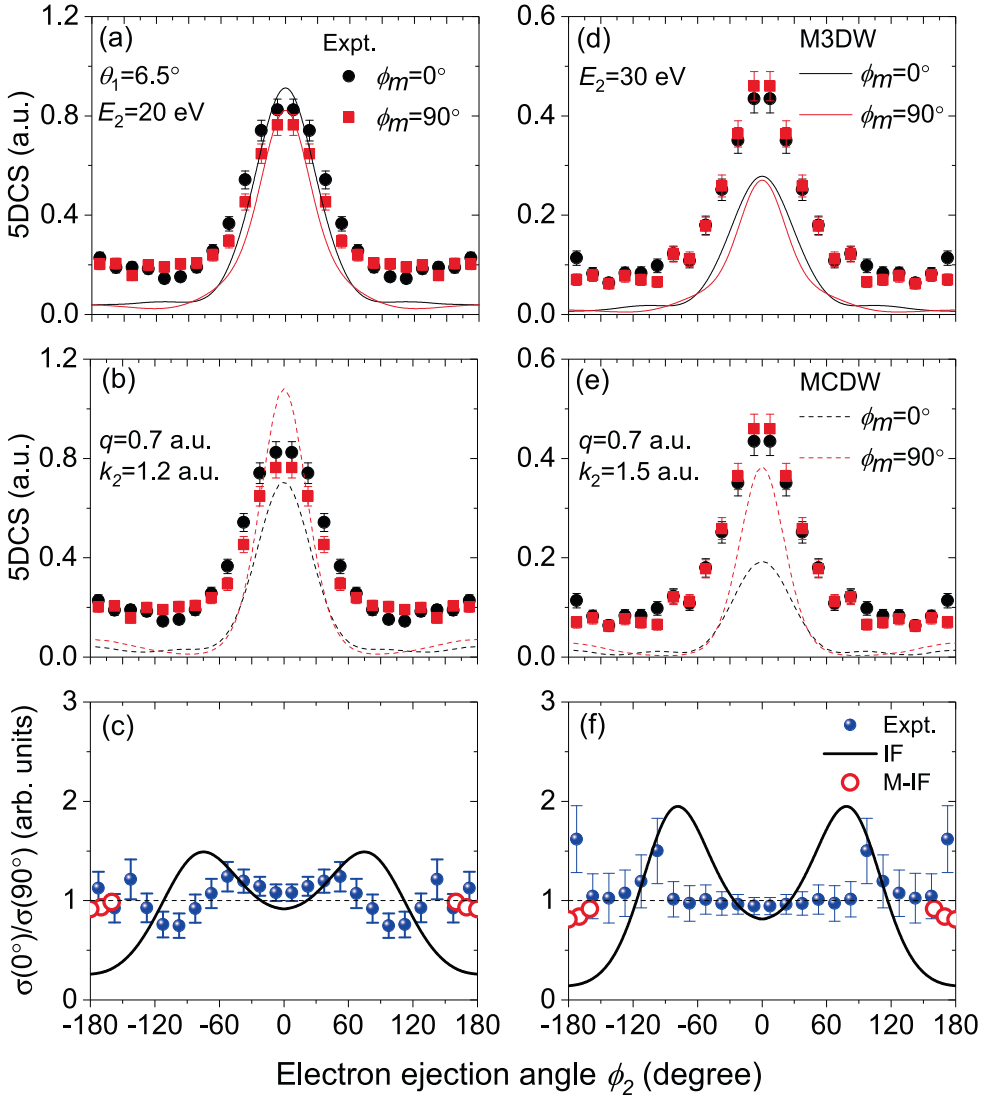

Fig. 2. Measured molecular-frame (e, 2e) cross sections of H_2 in the perpendicular plane in comparison with M3DW (top row) and MCDW (middle row) and the cross section ratios $\sigma_{H_2}(\phi_m = 0°)/\sigma_{H_2}(\phi_m = 90°)$ in the bottom row. The scattering angle is $\theta_1 = 6.5°$ and ejected energies are $E_2 = 20$ eV (left column) and $E_2 = 30$ eV (right column). The emission patterns at $\phi_2 \sim 0°$ and $\phi_2 \sim 180°$ correspond to the binary and recoil lobes, respectively. In (f), abbreviations IF and M-IF indicate interference model and modified interference model, respectively. The data for the M-IF model are only shown for angles $\phi_2 \sim 180°$ (for details see text).

In the following the 5DCSs as a function of the emission angle ϕ_2 are shown as Cartesian plots for better quantitative comparison. Figures 2–4 show results for the scattering angles of $\theta_1 = 6.5°$, 10° and 20°, respectively. Each figure displays data for $E_2 = 20$ eV (left columns) and $E_2 = 30$ eV (right columns). Since these perpendicular geometries show mirror symmetry with respect to the x–z planes, the experimental data were also mirrored with respect to $\phi_2 = 0°$. In the figures, the same experimental 5DCS are compared to the M3DW theory (top rows) and the MCDW theory (center rows), respectively for both molecular axis angles. Finally, the bottom rows are focused on the Young-type interference effect by comparing the cross section ratios between two molecular alignments ($\phi_m = 0°$ and $\phi_m = 90°$) with the interference model. While the experimental cross section data are not absolute, the different kinematics are measured in the same experimental run and, thus, are internormalized. Therefore, a single common factor is sufficient for normalization which was chosen by scaling the experimental data at $\theta_1 = 6.5°$, $E_2 = 20$ eV in the binary region to the M3DW calculation.

The 5DCSs exhibit a single binary peak at 0° and a small or even flat recoil lobe at 180° for all measured scattering angles and ejected energies. Comparing with the MCDW and the M3DW calculations, both qualitatively reproduce the binary peak in shape while the cross section in the recoil region is strongly underestimated. Since the

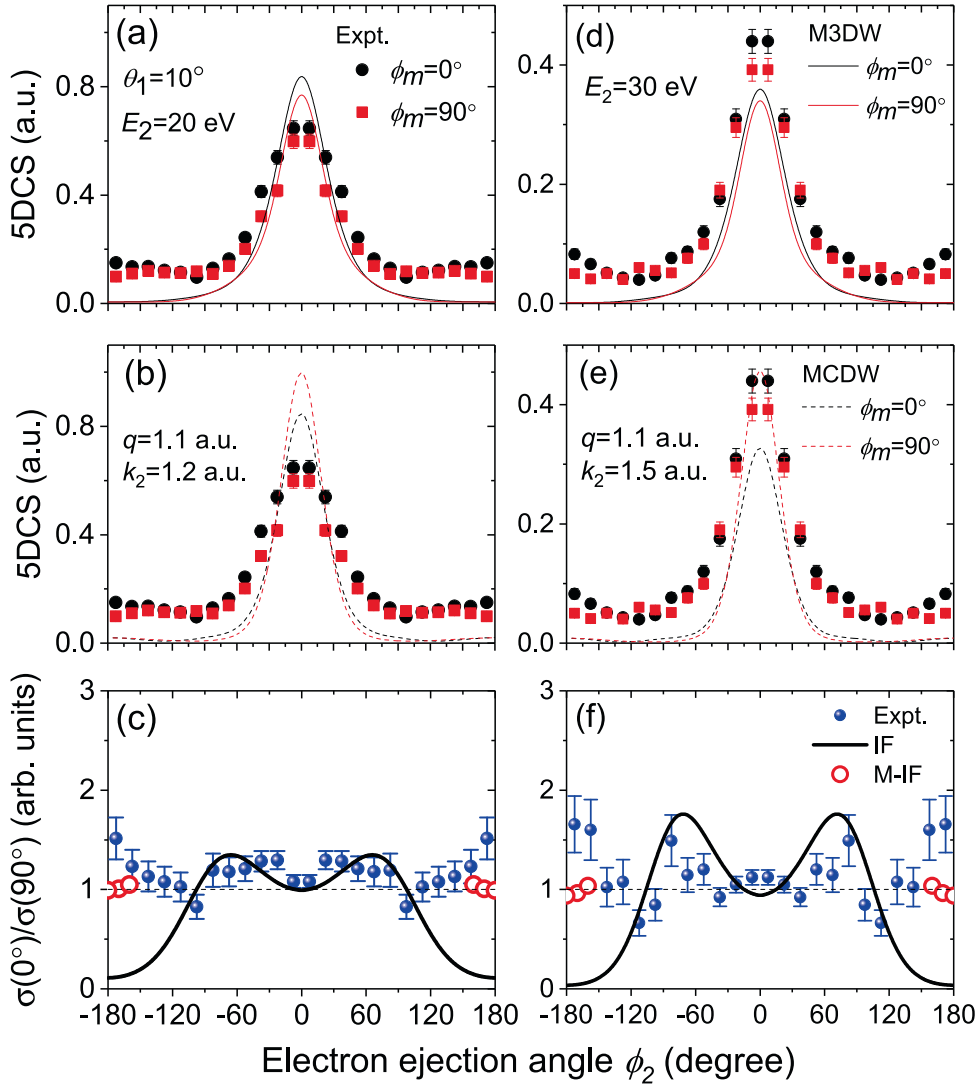

Fig. 3. Same as Figure 2 but for $\theta_1 = 10°$.

experimental data are internormalized the relative magnitudes of the 5DCSs can be compared between experiment and theories. The experimental data show similar magnitudes of the binary peaks for the scattering angles $\theta_1 = 6.5°$ and 10° and a significant decrease for 20° which is fairly well reproduced by both models for $E_2 = 20$ eV. For $E_2 = 30$ eV on the other hand the experimental cross sections decrease faster for increasing scattering angle θ_1 than predicted by theories.

In our previous studies for lower ejected electron energies of $E_2 = 10$ eV [36] and 18 eV [18] we observed significant higher cross section if the molecular axis was parallel to the emission direction $\phi_m = \phi_2$ as compared to perpendicular alignment. This was interpreted as deflection of the emitted electron in the anisotropic potential of the molecular ion and preferred emission along the molecular axis. In the present experimental data for $E_2 = 20$ eV we find qualitatively the same behavior although the molecular alignment dependence of the cross section is rather small. The cross sections in the vicinity of the binary and recoil peaks ($\phi_2 = 0°$, 180°) are slightly higher for $\phi_m = 0°$ compared to $\phi_m = 90°$. Consequently for $\phi_2 = 90°$ the cross section is higher around $\phi_m = 90°$ compared to $\phi_m = 0°$. For 30 eV these differences become even smaller and the data do not show persistently a significant alignment dependence outside the statistical error bars. This indicates a reduced distortion effect on the ejected electron if it has higher energy. The magnitude of the alignment dependence is roughly reproduced by the M3DW results while MCDW overestimates the differences in the binary peak region.

The experimental cross section ratios between two distinct molecular alignments are shown in the third row of the figures. This aims to verify Young-type interference effect in the electron emission patterns of aligned H_2 molecule. The cross section ratio $\tilde{R}$ based on the two-center interference (IF) model of equation (2) is presented as a black solid curve in the figures. As discussed above,

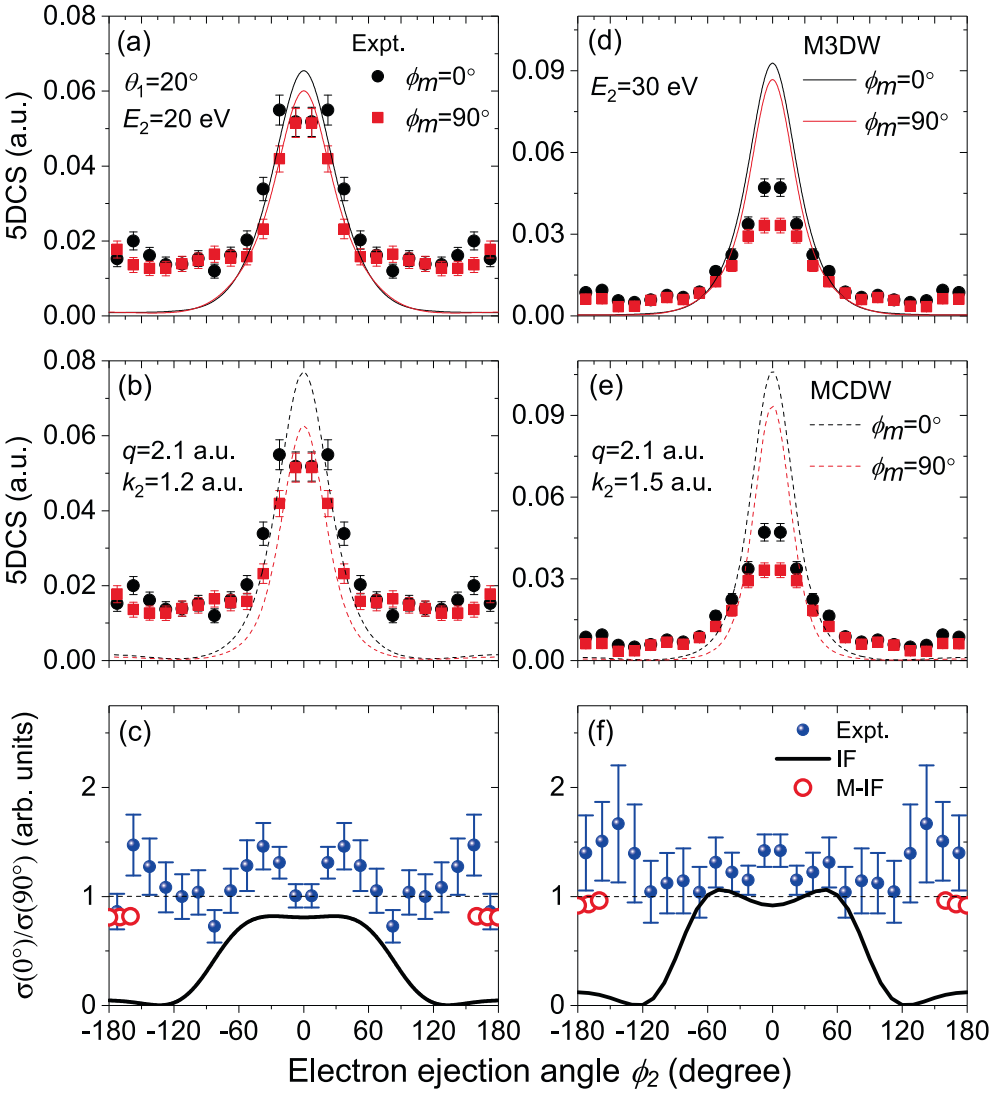

Fig. 4. Same as Figure 2 but for $\theta_1 = 20°$.

the atomic cross section cancels out in the ratio and the Young-type interference effects should be directly observable. It can be seen from Figures 2–4 that the experimental, and the IF ratios show more or less pronounced variations around the ratio 1. The behavior of the IF ratio $\tilde{R}$ can be understood from the cosine functions in equation (2). In the binary peak region $\phi_2 \approx 0$, the vector $\vec{k}_2 - \vec{q}$ is smallest in magnitude and it has a component parallel $\vec{R}_{\phi_m} = 0°$ while it is perpendicular to $\vec{R}_{\phi_m} = 90°$. Therefore, in equation (2) the cosine in the denominator is 1 while in the numerator it is close to but smaller than 1 resulting in the ratio $\tilde{R}$ being slightly smaller than 1. For increasing ϕ_2 the vector $\vec{k}_2 - \vec{q}$ rises in magnitude and quickly turns from being inside the x–z plane to angles roughly parallel to $\vec{R}_{\phi_m} = 90°$ such that the cosine in the denominator is smaller than 1 and $\tilde{R}$ becomes larger than 1. Finally for ϕ_2 around 180° the vector $\vec{k}_2 - \vec{q}$ is large and roughly parallel $\vec{R}_{\phi_m} = 0°$ such that the argument of the cosine in the numerator of equation (2) may approach or exceed $\pi/2$. As a result $\tilde{R}$ is close to zero.

Here we suggest a modification of the interference formula in the recoil region since it does not account for the physical mechanism underlying the recoil peak. As mentioned above, the recoil peak originates from backscattering of the outgoing ejected electron wave in the ionic potential. On the other hand the interference formula only considers direct electron emission into a particular direction. If backscattering occurs in the molecular ion potential as a whole then there is a sign change of the $\vec{k}_2 \cdot \vec{R}$ phase in formula equation (1) as illustrated in Figure 1d and elucidated in the following. $\vec{k}_2 \cdot \vec{R}$ is the phase difference of the emitted waves for direct emission of an electron with momentum $\vec{k}_2$. In case an electron observed in direction of $\vec{k}_2$ stems from backscattering it was initially emitted along $-\vec{k}_2$ with relative phase $-\vec{k}_2 \cdot \vec{R}$. For a subsequent backscattering in the molecular ion potential as a whole this phase persists such that it has opposite sign

compared to the waves directly emitted along the $\vec{k}_2$ direction. Therefore, in order to account for the backscattering in the interference formula of equation (1) for the recoil peak angular region around $\phi_2 \sim 180°$, we invert the outgoing electron momentum $\vec{k}_2 \rightarrow -\vec{k}_2$ such that the sign of the phase contribution $\vec{k}_2 \cdot \vec{R}$ changes while $\vec{q} \cdot \vec{R}$ is unchanged. In this way it is possible to illustrate how the final state electron-ion interaction can modify the interference pattern. Here the recoil peak is very small, not well separated from the binary peak and it is unclear how the transition from the regular to the modified interference model has to be described. Therefore, the resulting $\tilde{R}$ values of the modified IF are shown in the figures only for a small angular range $160° \leq \phi_2 \leq 180°$ (open circles labeled as M-IF).

From the results in the bottom rows of Figures 2–4, it is obvious that the $\tilde{R}$ predictions from the IF model are generally not a good description of the experimental data except in the binary peak where both show $\tilde{R}$ values close to 1. For the $E_2 = 20\,\text{eV}$ data there is a statistical significant oscillation around $\tilde{R} = 1$. Here for $\theta_1 = 10°$ (Fig. 3c) there is the best agreement in the angular range from $\phi_2 = 0°$ to $\sim 100°$ with a minimum at the binary peak and a maximum at $\phi_2 \sim 70°$. Nevertheless, for the recoil region the IF model strongly deviates from experiment. For $\theta_1 = 6.5°$ the maximum in the IF model is shifted to 80° while the experimental data show a maximum around 60° in Figure 2c. For $\theta_1 = 20°$ the agreement worsens concerning the magnitude of the cross section ratio (Fig. 4c). For all kinematics there is strong disagreement with the IF formula in the angular range of the recoil peak while the agreement with our modified IF model is improved. For higher energy $E_2 = 30\,\text{eV}$ the amplitude of the $\tilde{R}$ oscillations is larger for the IF model while experimentally they rather decrease (Figs. 2 and 4) or stay roughly unchanged (Fig. 3). These observations indicate that the experimental oscillations in the cross section ratios are rather not dominated by the two-wave interference which underlies the IF formula but are likely due to the scattering of the ejected electron in the two-center ionic potential. Here we do not discuss the cross-section ratios for the two theoretical models since they obtain very small cross sections outside the binary peak region. As a consequence the ratios $\tilde{R}$ show oscillations with large amplitude and a comparison with experiment is not meaningful.

5 Conclusion

In summary, we performed a molecular-frame (e, 2e) experiment of H_2 at 520 eV impact-energy. The fivefold differential cross sections (5DCS) were obtained in the perpendicular plane for two molecular alignments of H_2 perpendicular to each other. The experimental data were internormalized across all measured scattering angles and ejected energies. The 5DCSs were compared to predictions from the multi-center distorted-wave (MCDW) as well as the molecular three-body distorted wave (M3DW) approaches. These methods use rather accurate molecular-frame bound state wave functions. On the other hand both models apply different approximations to describe propagation of the continuum waves in the molecular potential. The M3DW model uses spherically symmetrised potentials for obtaining the distorted waves in the initial and final states. The ejected electron in the MCDW model is described utilizing a multi-center potential of the molecular ion which principally can give rise to coupling between different angular momenta of the ejected electron. Yet the respective non-diagonal matrix elements are neglected in order to make the calculation feasible [42,43].

Both models consider the molecule as an effective one electron system neglecting, e.g. interchannel coupling and partially ground state correlation. If normalized to the experimental binary peak the theoretical 5DCS strongly underestimate the cross section in the remaining angular range and in particular in the recoil peak region where distortion and backscattering effects are important. Concerning the alignment dependent variations of the 5DCS, these are found to be fairly small for $E_2 = 20\,\text{eV}$ and close to statistically insignificant at 30 eV. Here, M3DW is in better agreement with experiment than MCDW which overestimates the alignment dependent differences in the binary peak region. It is to be noted that the present calculations are far from satisfactory for reproducing the experimental results. Possible reasons are the spherically symmetric distortion potential in M3DW and the above mentioned missing non-diagonal matrix elements in MCDW [42,43]. Therefore, both models do not account for angular momentum exchange between the ejected electron and the molecular ion. In order to enhance its accuracy and to overcome part of its shortcomings the MCDW theory is presently extended to include coupling of different partial waves of the ionized electron.

In order to investigate possible interference patterns, we presented 5DCS ratios $\tilde{R}$ between two different orthogonal molecular alignments. In this way, the atomic cross section cancels out and if present the pure two-center molecular effects in the (e, 2e) reaction should become visible. It was found that the ratios are close to the predicted two-center interference pattern only in the binary region and for the $|q| \approx |k_2|$ kinematics, i.e. in the direct binary-collision processes. For the recoil peak we suggested a modified interference factor which takes into account the backscattering process leading to the recoil peak which gives better agreement with the experimental value at $\phi_2 \approx 180°$.

One has to conclude that the present kinematics are not appropriate to fully reveal the two-center interference for the (e, 2e) reaction on H_2 which requires undisturbed electron emission from the two atomic centers. While the projectile energy of 520 eV should be sufficiently high to prevent significant mutual interaction of the ionized and scattered electrons (post collision interaction) the ionized electron energy is rather low such that the respective outgoing wave is distorted by the ionic two-center potential. Clearly still higher energies E_2 (above 100 eV) are required to come closer to an undistorted outgoing wave for the ionized electron [50]. In the present experiment we could not obtain 5DCS for higher energy E_2 due to the strongly dropping cross section for increasing E_2 while the projectile beam current was limited by the total detector count rate which is mainly determined by the abundant

low energy electrons. In future we aim to overcome this limitation by implementing additional electron detectors which are only reached by the faster ionized electrons.

Open access funding provided by Projekt DEAL. The work was jointly supported by the National Natural Science Foundation of China under grant Nos. 11774281, 11534011 and 11974272, the National Key Research and Development Program of China under grant No. 2017YFA0402300, and the Deutsche Forschungsgemeinschaft (DFG) project under grant No. RE 2966/3-1. E.W. acknowledges a fellowship from the Alexander von Humboldt Foundation.

Author contribution statement

X.R., E.W. and A.D. performed the experiments and analyzed the data. E.A. and D.M. carried out the M3DW calculations. X.L. and X.C. carried out the MCDW calculations. E.W., X.R. and A.D. wrote the first draft of the manuscript. All authors contributed to the final version of the manuscript.

References

1. M.A. Huels, B. Boudaiffa, P. Cloutier, D. Hunting, L. Sanche, J. Am. Chem. Soc. **125**, 4467 (2003)
2. K. Bartschat, M.J. Kushner, Proc. Natl. Acad. Sci. (USA) **113**, 7026 (2016)
3. H. Ehrhardt, K. Jung, G. Knoth, P. Schlemmer, Z. Phys. D: At. Mol. Clusters **1**, 3 (1986)
4. A. Lahmam-Bennani, J. Phys. B: At. Mol. Opt. Phys. **24**, 2401 (1991)
5. T.N. Resigno, M. Baertschy, W.A. Isaacs, C.W. McCurdy, Science **286**, 2474 (1999)
6. I. Bray, Phys. Rev. Lett. **89**, 273201 (2002)
7. J. Colgan, M.S. Pindzola, F.J. Robicheaux, D.C. Griffn, M. Baertschy, Phys. Rev. A **65**, 042721 (2002)
8. I. Bray, D. Fursa, A. Kadyrov, A. Stelbovics, A. Kheifets, A. Mukhamedzhanov, Phys. Rep. **520**, 135 (2012)
9. J. Colgan, M. Foster, M.S. Pindzola, I. Bray, A.T. Stelbovics, D.V. Fursa, J. Phys. B: At. Mol. Opt. Phys. **42**, 145002 (2009)
10. O. Zatsarinny, K. Bartschat, Phys. Rev. Lett. **107**, 023203 (2011)
11. X. Ren, A. Senftleben, T. Pflüger, K. Bartschat, O. Zatsarinny, J. Berakdar, J. Colgan, M.S. Pindzola, I. Bray, D.V. Fursa, A. Dorn, Phys. Rev. A **92**, 052707 (2015)
12. T. Pflüger, O. Zatsarinny, K. Bartschat, A. Senftleben, X. Ren, J. Ullrich, A. Dorn, Phys. Rev. Lett. **110**, 153202 (2013)
13. X. Ren, S. Amami, O. Zatsarinny, T. Pflüger, M. Weyland, W.Y. Baek, H. Rabus, K. Bartschat, D. Madison, A. Dorn, Phys. Rev. A **91**, 032707 (2015)
14. X. Ren, S. Amami, O. Zatsarinny, T. Pflüger, M. Weyland, A. Dorn, D. Madison, K. Bartschat, Phys. Rev. A **93**, 062704 (2016)
15. M. Takahashi, N. Watanabe, Y. Khajuria, Y. Udagawa, J.H.D. Eland, Phys. Rev. Lett. **94**, 213202 (2005)
16. S. Bellm, J. Lower, E. Weigold, D.W. Mueller, Phys. Rev. Lett. **104**, 023202 (2010)
17. A. Senftleben, T. Pflüger, X. Ren, O. Al-Hagan, B. Najjari, D. Madison, A. Dorn, J. Ullrich, J. Phys. B: At. Mol. Opt. Phys. **43**, 081002 (2010)
18. X. Ren, T. Pflüger, S. Xu, J. Colgan, M.S. Pindzola, A. Senftleben, J. Ullrich, A. Dorn, Phys. Rev. Lett. **109**, 123202 (2012)
19. J. Colgan, M.S. Pindzola, F. Robicheaux, C. Kaiser, A.J. Murray, D.H. Madison, Phys. Rev. Lett. **101**, 233201 (2008)
20. M.C. Zammit, J.S. Savage, D.V. Fursa, I. Bray, Phys. Rev. Lett. **116**, 233201 (2016)
21. H.D. Cohen, U. Fano, Phys. Rev. **150**, 30 (1966)
22. N. Stolterfoht, B. Sulik, V. Hoffmann, B. Skogvall, J.Y. Chesnel, J. Rangama, F. Frémont, D. Hennecart, A. Cassimi, X. Husson, A.L. Landers, J.A. Tanis, M.E. Galassi, R.D. Rivarola, Phys. Rev. Lett. **87**, 023201 (2001)
23. D. Misra, U. Kadhane, Y.P. Singh, L.C. Tribedi, P.D. Fainstein, P. Richard, Phys. Rev. Lett. **92**, 153201 (2004)
24. D. Rolles, M. Braune, S. Cvejanovic, O. Geßner, R. Hentges, S. Korica, B. Langer, T. Lischke, G. Prümper, A. Reinköster, J. Viefhaus, B. Zimmermann, V. McKoy, U. Becker, Nature **437**, 711 (2005)
25. D. Akoury, K. Kreidi, T. Jahnke, T. Weber, A. Staudte, M. Schoffer, N. Neumann, J. Titze, L.P.H. Schmidt, A. Czasch, O. Jagutzki, R.A.C. Fraga, R.E. Grisenti, R.D. Muino, N.A. Cherepkov, S.K. Semenov, P. Ranitovic, C.L. Cocke, T. Osipov, H. Adaniya, J.C. Thompson, M.H. Prior, A. Belkacem, A.L. Landers, H. Schmidt-Bocking, R. Dorner, Science **318**, 949 (2007)
26. X.-J. Liu, N.A. Cherepkov, S.K. Semenov, V. Kimberg, F. Gelmukhanov, G. Prümper, T. Lischke, T. Tanaka, M. Hoshino, H. Tanaka, K. Ueda, J. Phys. B **39**, 4801 (2006)
27. S.E. Canton, E. Plesiat, J.D. Bozek, B.S. Rude, P. Decleva, F. Martin, Proc. Natl. Acad. Sci. (USA) **108**, 7302 (2011)
28. Z. Zhang, X. Shan, T. Wang, E. Wang, X. Chen, Phys. Rev. Lett. **112**, 023204 (2014)
29. M.F. Ciappina, O.A. Fojón, R.D. Rivarola, J. Phys. B: At. Mol. Opt. Phys. **47**, 042001 (2014)
30. C.R. Stia, O.A. Fojón, P.F. Weck, J. Hanssen, R.D. Rivarola, J. Phys. B **36**, L257 (2003)
31. A. Senftleben, O. Al-Hagan, T. Pflüger, X. Ren, D. Madison, A. Dorn, J. Ullrich, J. Chem. Phys. **133**, 044302 (2010)
32. A.J. Murray, J. Phys. B: At. Mol. Opt. Phys. **38**, 1999 (2005)
33. D.S. Milne-Brownlie, M. Foster, J. Gao, B. Lohmann, D.H. Madison, Phys. Rev. Lett. **96**, 233201 (2006)
34. E.M.S. Casagrande, A. Naja, F. Mezdari, A. Lahmam-Bennani, P. Bolognesi, B. Joulakian, O. Chuluunbaatar, O. Al-Hagan, D.H. Madison, D.V. Fursa, I. Bray, J. Phys. B: At. Mol. Opt. Phys. **41**, 025204 (2008)

35. Z.N. Ozer, H. Chaluvadi, M. Ulu, M. Dogan, B. Aktas, D. Madison, Phys. Rev. A **87**, 042704 (2013)
36. X. Li, X. Ren, K. Hossen, E. Wang, X. Chen, A. Dorn, Phys. Rev. A **97**, 022706 (2018)
37. J.-Y. Chesnel, D. Martina, P. Sobocinski, O. Kamalou, F. Frémont, J. Fernández, F. Martýn, Phys. Rev. A **70**, 010701(R) (2004)
38. J. Ullrich, R. Moshammer, A. Dorn, R. Dörner, L.P.H. Schmidt, H. Schmidt-Böcking, Rep. Prog. Phys. **66**, 1463 (2003)
39. M. Dürr, C. Dimopoulou, B. Najjari, A. Dorn, J. Ullrich, Phys. Rev. Lett. **96**, 243202 (2006)
40. A. Senftleben, T. Pflüger, X. Ren, B. Najjari, A. Dorn, J. Ullrich, J. Phys. B **45**, 021001 (2012)
41. R.N. Zare, J. Chem. Phys. **47**, 204 (1967)
42. S. Zhang, X. Li, J. Wang, Y. Qu, X. Chen, Phys. Rev. A **89**, 052711 (2014)
43. X. Li, M. Gong, L. Liu, Y. Wu, J. Wang, Y. Qu, X. Chen, Phys. Rev. A **95**, 012703 (2017)
44. J. Gao, D.H. Madison, J.L. Peacher, A.J. Murray, M.J. Hussey, J. Chem. Phys. **124**, 194306 (2006)
45. D.H. Madison, O. Al-Hagan, J. At. Mol. Opt. Phys. **2010**, 24 (2010)
46. E. Ali, K. Nixon, A. Murray, C. Ning, J. Colgan, D. Madison, Phys. Rev. A **92**, 042711 (2015)
47. G.W. Drake, ed., *Atomic, Molecular and Optical Physics* (Springer Science, 2006)
48. B. Bransden, C. Joachain, in *Physics of Atoms and Molecules* (Longman Group Limited, 1983), p. 515
49. M.J. Frisch, G.W. Trucks, H.B. Schlegel, G.E. Scuseria, M.A. Robb, J.R. Cheeseman, G. Scalmani, V. Barone, G.A. Petersson, H. Nakatsuji, X. Li, M. Caricato, A.V. Marenich, J. Bloino, B.G. Janesko, R. Gomperts, B. Mennucci, H.P. Hratchian, J.V. Ortiz, A.F. Izmaylov, J.L. Sonnenberg, D. Williams-Young, F. Ding, F. Lipparini, F. Egidi, J. Goings, B. Peng, A. Petrone, T. Henderson, D. Ranasinghe, V.G. Zakrzewski, J. Gao, N. Rega, G. Zheng, W. Liang, M. Hada, M. Ehara, K. Toyota, R. Fukuda, J. Hasegawa, M. Ishida, T. Nakajima, Y. Honda, O. Kitao, H. Nakai, T. Vreven, K. Throssell, J.A. Montgomery, Jr., J.E. Peralta, F. Ogliaro, M.J. Bearpark, J.J. Heyd, E.N. Brothers, K.N. Kudin, V.N. Staroverov, T.A. Keith, R. Kobayashi, J. Normand, K. Raghavachari, A.P. Rendell, J.C. Burant, S.S. Iyengar, J. Tomasi, M. Cossi, J.M. Millam, M. Klene, C. Adamo, R. Cammi, J.W. Ochterski, R.L. Martin, K. Morokuma, O. Farkas, J.B. Foresman, D.J. Fox, *Gaussian 16 Revision A.03* (Gaussian Inc., Wallingford CT, 2016)
50. L. Avaldi, R. Camilloni, E. Fainelli, G. Stefani, J. Phys. B: At. Mol. Phys. **20**, 4163 (1987)